PHOTONICS Research

Tunable narrowband antireflection optical filter with a metasurface

Luigi Bibbò, Karim Khan, Qiang Liu, Mi Lin, Qiong Wang, and Zhengbiao Ouyang*

College of Electronic Science and Technology of Shenzhen University, THz Technical Research Center of Shenzhen University, Key Laboratory of Optoelectronics Devices and Systems of Ministry of Education and Guangdong Province, Shenzhen University, Shenzhen 518060, China
**Corresponding author: zbouyang@szu.edu.cn*

Received 9 June 2017; revised 21 August 2017; accepted 22 August 2017; posted 6 September 2017 (Doc. ID 297784); published 27 September 2017

A narrowband tunable antireflection optical filter is proposed and numerically studied. The structure is a metasurface based on plasmonic nanoparticles on an electro-optic film in a three-layer configuration of metal-dielectric-metal (MDM) in the visible near-infrared range. By tuning the voltage and thus tuning the refractive index of the dielectric $LiNbO_3$, one can shift the wavelength of minimum reflection as desired. The parameters of gold nanoparticles and other elements used for the filter design and refractive index of the dielectric are obtained by the finite-element method (FEM). An analytical theory is presented to explain the FEM simulation results, and they agree well with each other. It is found that the frequency of the plasmonic resonance wave on the metasurface should be equal to that of the Fabry–Perot resonator formed by the MDM to have a good filtering property. Theoretical spectra obtained by FEM simulation show that the structure has extensive potential for the design of tunable narrow-band filters for modulators, displayers, and color extraction for imaging.

OCIS codes: (120.2440) Filters; (230.2090) Electro-optical devices; (240.6680) Surface plasmons; (160.3918) Metamaterials.

https://doi.org/10.1364/PRJ.5.000500

1. INTRODUCTION

A narrowband antireflection optical filter (NAOF) is a filter that has a nearly zero-reflection narrow band within a wide bandgap region where high reflection occurs. The NAOF is useful for eliminating an interfering signal with a fixed frequency. When the filtering frequency is made tunable, various applications, e.g., frequency varying anti-interference filtering, optical switching, modulation, demodulation, and sensing, can be achieved. Conventionally, an NAOF can be realized by forming a defect (layer defect or point defect) in a multilayer photonic crystal (PhC) [1]. Although PhCs have subwavelength properties, a PhC with a defect layer is still relatively large, and it can decrease the degree of integrations in micro-optical devices. Furthermore, this system imposes strict requirements on the defect, including the refractive index and thickness of the defect, as well as complex fabrication processes that make it difficult to integrate into micro-optical systems. Therefore, NAOFs with smaller size have to be developed.

Surface plasmons (SP), metasurfaces (which are ultrathin layers of metamaterial), and related nanostructures, with their special properties to localize light in a subwavelength scale with high local field enhancement, indicating a wide range of applications—including optical trapping, energy harvesting, biosensing, spectral filter, absorbers [2–5]—introduce a way for developing smaller NAOFs. Especially of great interest are metasurface structures based on metal nanospheres coupled to metal layers separated by a dielectric layer, known as a metal-dielectric-metal (MDM) structure, which is called by another name, i.e., metal-insulator-metal (MIM), in electronics. Metasurfaces of this kind were intensively studied to provide a new solution to traditional optical processes such as spectral filtering, as an alternative to nanoholes or periodic grooves [6,7] or defective PhCs [8] or nanodisk resonators [9,10]. Metasurfaces have attracted much interest for their use in many frequency domains as surface wave couplers [11], flat lenses [12], polarization control [13], and holograms [14].

The design of a planar structure based on a set of resonant meta-atoms with distinct electromagnetic (EM) responses has a limit because it can work only for a single frequency.

The meta-atoms exhibit a linear phase profile only at a frequency f_0, while at another frequency they have phase dispersion with consequent degradation of device performance.

The performance depends on the EM response of the passive meta-atoms and is thus strongly related to the working frequency [15]. Xu *et al.* have overcome this limit, realizing a tunable metasurface (TMS) with meta-atoms controlled by external voltage. By introducing a varactor diode into meta-atoms and applying a voltage on the diode, it is possible to

control the reflection phase of meta-atoms, so that the phase profile of meta-atoms remains linear and the device can work in a large frequency band [16,17].

The limit of all planar metasurfaces based on passive resonant meta-atoms used for phase or amplitude modulation is the intrinsic dispersion that the performance outside the working frequency deteriorates, and it avoids changing the functionality. To overcome the problem, it is possible to employ a varactor diode to tune the resonant frequencies by varying the voltage applied.

The voltage applied causes the capacitance change and then the frequency with consequent change of reflection phase spectrum. This solution has been adopted by Xu *et al.* for the realization of aberration-free and functionality-switchable metalenses with tunable focal length in the microwave range [18].

The same author, also using a varactor diode, has realized a device that is able to manipulate the polarization state of EM waves [19]. It is composed of a TMS, including a circularly polarized (CP) helicity converter, helicity hybridizer, and helicity keeper, which can dynamically switch its functionality on helicity control of CP waves behaving as a helicity converter and helicity hybridizer with two separate frequency bands in the "ON" state and become a helicity keeper with an ultrawide band in the "OFF" state.

The filter function of these structures is due to SPs propagating along the metal–dielectric interface. Plasmonic structures exhibit interesting features such as the ability to enhance EM fields within a broad range of optical frequencies, the ability in manipulating the operating bandwidth by controlling the geometrical parameters of nanoparticles (instead of exclusively using the optical properties of materials), and simplicity in structure for transferring from the laboratory stage to the manufacturing stage. In previous work, two different types of Bragg reflectors, the MIM or insulator-metal-insulator (IMI) plasmonic waveguides, were used [20,21]. For the two structures, the MIM waveguide is preferred for integration in optical circuits for its strong confinement of light and acceptable propagating length of SP. Therefore, we build the NAOF based on MDM, similar to MIM, because the dielectric used is $LiNbO_3$, which is an electric insulator. The MDM itself forms a Fabry–Perot resonator, and resonant absorption can occur at the resonance wavelength, and thus an NAOF can be realized.

Adding tunability to filters is attractive, as it generates a lot of applications. Previously the tunability of filters has been done thermo-optically [22], by changing the angle of incident light, or by changing the lattice parameters [23,24]. But these structures are not compact and are difficult to integrate with electronic circuits. In this work, the tunability is realized by using an electro-optic (EO) material, inserted above the substrate, whose refractive index can be varied via the Pockels effect by applying an electric field. In this way, the effective resonator length and thus the resonance wavelength of the NAOF can be tuned by varying the electric field applied.

The innovative aspect of the work was to have combined the plasmonic resonance on the metasurface with tunable Fabry–Perot resonance absorption properties through the help of an EO layer in the structure, resulting a tunable narrowband antireflection filter. The device can have ultrafast operational speeds and is easily integrated into optical circuits.

2. PHYSICAL MODEL

The proposed plasmonic NAOF is based on an MDM structure in which the unit cell consists of three layers formed by a top layer of a gold nanoparticle array placed on the same plane embedded in dielectric layer and a metal ground substrate [25]. Figure 1 shows the schematic structure of the proposed NAOF, which consists of 12 nm radius nanospheres, where the spheres are spaced in a unit cell of 100 nm. The centers of the three spheres in the unit cell form an isoceles triangle whose base line and altitude normal to the base line are 40 and 30 nm, respectively. Thickness of the dielectric spacer is 70 nm, and thickness of metallic substrate is 420 nm. The material chosen for the nanoparticles array and bottom substrate is gold whose permittivity can be derived from Drude-Lorentz:

$$\varepsilon_{rAu} = \varepsilon_\infty - \omega_p^2/(\omega^2 - j\gamma\omega), \tag{1}$$

where $\varepsilon_\infty = 9$ is the permittivity at high frequency, $\omega_p = 1.37 \times 10^{16}$ rad/s is the plasma frequency, and $\gamma = 1.23 \times 10^{14}$ rad/s is the electron collision frequency.

The dielectric layer is $LiNbO_3$ [26], which is crystalline solid. It is electrically insulating with a bandgap of 4.0 eV with Curie temperature of 1142°C higher than the fusion temperature of 1253°C [27].

$LiNbO_3$ has high nonlinear optical and EO properties, including negative birefringence, two refractive indices, two ordinary optical axes, which are set along the x axis and y axis, and an extraordinary optical axis along the z axis in the following. These indices are affected by temperature and dopants. It has another important property: The refractive index also can vary subjected to a nonhomogeneous illumination of visible light. Moreover, with the application of an external electric field, its ordinary refractive index can be written out as [28]

$$n_o = n_{o0} + 0.5 n_o^3 \gamma_{13} E, \tag{2}$$

where $n_{o0} = 2.30$ is the ordinary refractive index of $LiNbO_3$ for the zero applied electric field, $\gamma_{13} = 10$ pm/V is the EO coefficient, $E = V/h_1$ is the applied electric field with V and h_1 being the voltage and the thickness of the EO layer. Although the extraordinary refractive index also varies with the applied voltage; however, we suppose the input wave has

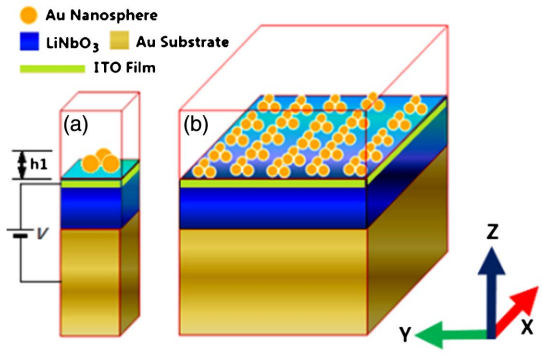

Fig. 1. (a) Unit cell with three spheres on the same plane in triangular configuration. (b) Overview schematic of the designed structure.

a polarization along the x axis; thus, it does not influence the propagation of the wave. In simulations, a plane wave is supposed to come from top.

Coupled mode theory can be used to theoretically analyze [29]. However, here we present a simple theoretical analysis in Section 4 for explaining the results shown in Section 3. To study the optical properties of the structure, we have used the FEM simulation tool: COMSOL MULTIPHYSICS.

3. SIMULATION AND RESULTS

By simulation we obtain the reflection and absorption spectra, which are shown in Fig. 2. From Fig. 2 we can see a deep narrow small reflection band, which can be used for narrowband antireflection filtering.

We mention that we had studied different configurations but found that the triangular configuration displays better performance.

To look into the mechanism behind the optical response indicated in Fig. 2, the electric and magnetic field distributions at the resonance wavelength of 623.29 nm are displayed in Figs. 3(a) and 3(b), respectively, while those at a nonresonance wavelength are displayed in Figs. 3(c) and 3(d), respectively. Comparing Figs. 3(a) and 3(b) with Figs. 3(c) and 3(d), respectively, we can see that, at resonance, there is no reflected wave, and there are strong surface modes around the nanospheres, while at nonresonance the reflection is high. The results confirm that there exists resonance absorption. Moreover, from Fig. 3 we can see that the fields are localized and enhanced around the nanoparticles, confirming that the SP can only exist on the surface. The field enhancement is achieved by the charge induction between the particles [30]. The strong fields around the nanospheres can be regarded as plasmonic resonance because the metasurface and thus the surface field is periodic in two dimensions; thus, along the surface one can see a plasmonic standing wave, which is equivalent to a resonant wave in a cavity. At the same time, there is resonance in the MDM Fabry–Perot resonator. Due to the resonances, the waves spend more time on the surface of the spheres, leading to more power loss to the waves, which therefore explains the narrowband antireflection phenomenon. Furthermore, the other peaks of absorption in Fig. 2 can be explained by resonance frequency splitting due to strong coupling of resonant waves between the plasmonic surface modes and the Fabry–Perot resonance modes.

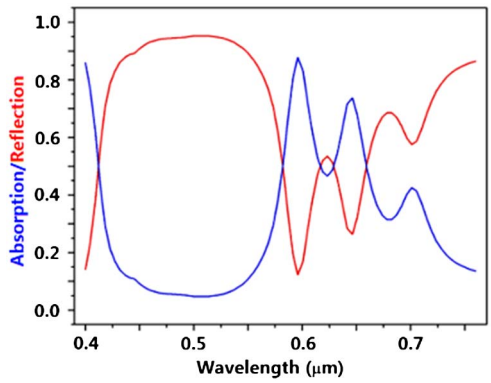

Fig. 2. Reflection and absorption spectra.

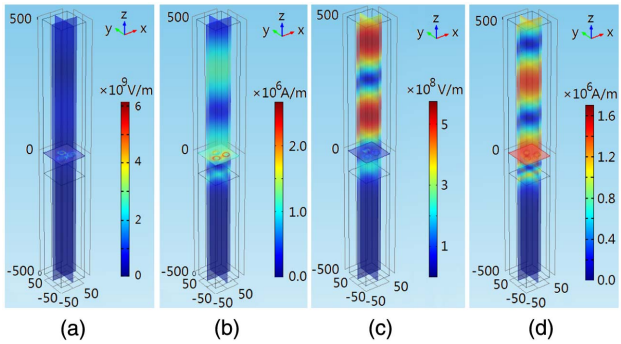

Fig. 3. (a) Electric field for wavelength of 623.29 nm. (b) Magnetic field for wavelength of 623.29 nm. (c) Electric field for wavelength of 550.38 nm. (d) Magnetic field for wavelength of 550.38 nm. The external electric applied is $V = 160$ V, and the dielectric refractive index is $n_o = 2.38$.

We also have studied the influence of the gold nanosphere radius, as shown in Fig. 4, for which the applied voltage is chose as 0. In Fig. 4(a), there is a large flat reflection band because the spheres are too small that their effects can be ignored, and the reflection is generated by the gold substrate. A better result for filtering is from the structure with a radius of 12 nm, as shown in Fig. 4(b), where the filter bandwidth is the narrowest. From Figs. 4(b) and 4(c), we can see that the filtering bandwidth increases as the nanosphere radius increases, and the structure can be regarded as a long wavelength absorber or short-wavelength reflector for Fig. 4(d). Therefore, the nanosphere radius also influences the sensitivity (S) and figure of merit (FOM) of the structure. To limit the influence of nanosphere radius, two sieves can be used in the fabrication process. One sieve has holes with radius r_1 slightly greater than the required radius r of the nanospheres and the other sieve has holes with radius r_2 slightly smaller than r. We can first screen out spheres with

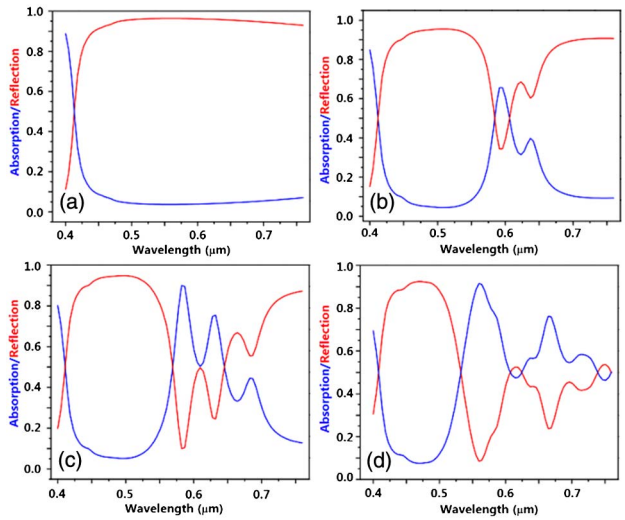

Fig. 4. Reflection and absorption spectra for different nanosphere radius: (a) 5 nm; (b) 12 nm; (c) 15 nm; and (d) 20 nm.

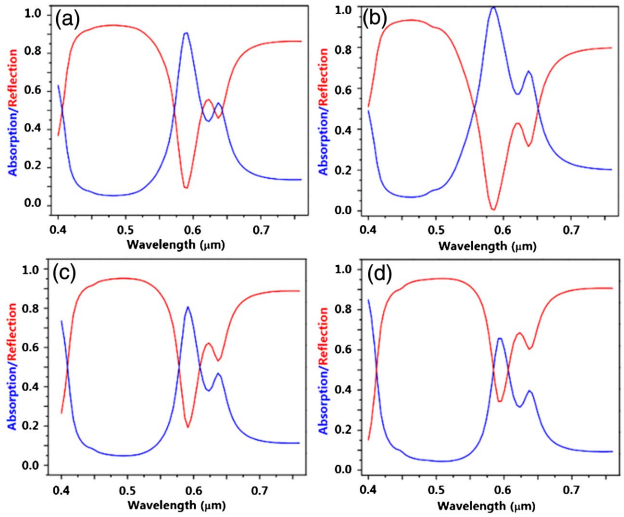

Fig. 5. Absorption and reflection versus wavelength for different dielectric thickness: (a) 60 nm; (b) 70 nm; (c) 75 nm; (d) 80 nm.

radii greater than r_1 and then screen out spheres with radii less than r_2, then we can obtain nanospheres with a very small dispersion of radius. Furthermore, to avoid the randomness in the position of nanospheres in the structure, we can use a template and glue to fix the spheres.

Similarly, we have analyzed the influence of dielectric thickness on the optical performance, while leaving the other parameters unchanged, as shown in Fig. 5, for which the applied voltage is chose as 0.

From Fig. 5, we can see that the dielectric thickness is an important factor, which has an evident influence on the absorption intensity at resonance. Fortunately, the fabrication precision can be lowered, as the effective dielectric thickness can be compensated by adjusting the electric voltage applied. We found an optimum filter performance for the dielectric thickness of 70 nm with a strong resonance absorption at 580 nm, as seen in Fig. 5(b). This optimum thickness is governed by the resonance condition given by Eq. (7). Without specifications, this value of dielectric thickness is used in the following.

Considering the response of metasurface relies on the geometry, size of the model and in particular on gold nanoparticles, in the realization stage the process of laser ablation can be used for the fabrication and size control of gold nanoparticles [31].

We also analyzed the optical response to the incidence angle [Figs. 6(a) and 6(b)]. The results obtained show that the influence of incidence angle is small, and it is almost incidence-angle independent for the value from 0° to 45°. This

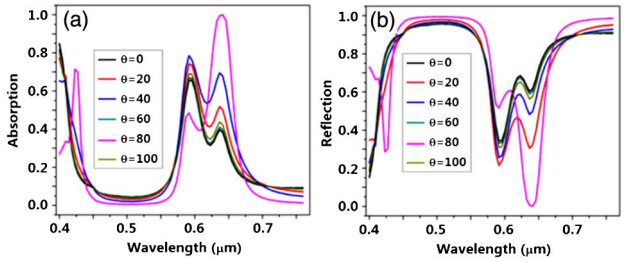

Fig. 6. (a) Absorption and (b) reflection to incident angle.

provides an important advantage in that one can directly act on the refractive index of the dielectric to obtain the desired filtering wavelength.

To get a clear idea of the effects of the dielectric's refractive index variation, an external electric field is applied to the structure, which is done via producing the optical spectra indicated in Fig. 7. The results obtained indicate a shift of filtering wavelength toward the longer wavelength region. Noting Eq. (2) and the relation between applied electric field E and the applied voltage $V = Eh_1$, where h_1 is the distance between the anode and the cathode, we can see that the refractive index and thus the effective thickness of the dielectric increases as the applied voltage increases, which means that the resonance wavelength of the Fabry–Perot resonator increases with the applied voltage, giving an explanation to the results obtained.

Figure 7 shows that, when the voltage changes from 0 to 160 V (the refractive index increases from 2.30 to 2.38, correspondingly), the filtering wavelength linearly shifts from 580 to 640 nm. This is understandable because the Fabry–Perot resonance wavelength to the effective cavity length, the effective cavity length to the dielectric refractive index, and the dielectric refractive index to the voltage applied, are

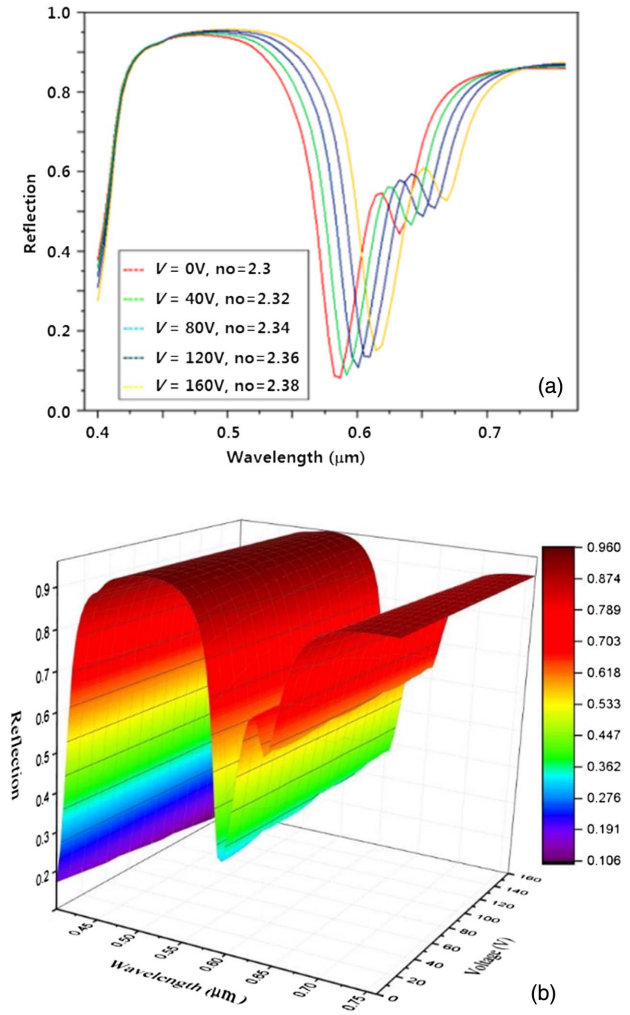

Fig. 7. (a) Optical spectra produced by the variation of applied voltage. (b) Optical spectra produced by applied voltage.

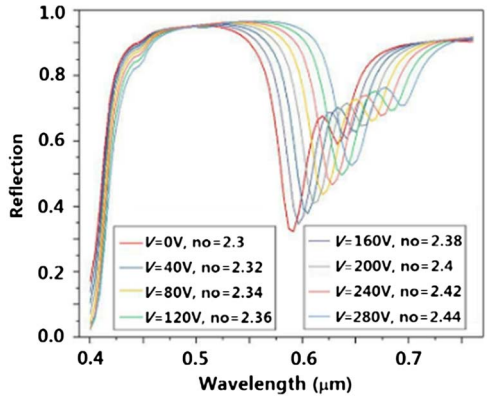

Fig. 8. Optical spectra for wider voltage range.

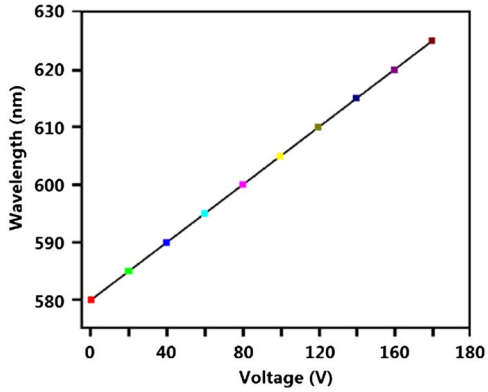

Fig. 9. Wavelength versus voltage.

all directly proportional; therefore, the resonance wavelength should be proportional to the applied voltage. To analyze the influence of applied voltage, the range has been enlarged until 280 V, as shown in Fig. 8. We can see that the filter also works at higher voltages. However, for best performance and frequency range of interest, the voltage range of 0–160 V is preferred. From Fig. 8, we can extract the relation between the filtering wavelength and the applied voltage, as displayed in Fig. 9 showing a perfect linear relation.

The dependence of reflection wavelength from refractive index of the spacer can ensure the narrowband antireflection filtering of the device [12]. The basic parameters of the filter are the tuning sensitivity (S) and FOM, which are, respectively, 0.25 nm/V and 0.0125 calculated from

$$S = \Delta\lambda/\Delta V, \tag{3}$$

$$\mathrm{FOM} = S/\mathrm{FWHM}, \tag{4}$$

where $\Delta\lambda$ is the resonance wavelength change, ΔV is voltage change, and FWHM is the full width at the half maximum of spectrum.

4. DISCUSSION

These relatively high values associated with the hypothesized structure parameters allow us to believe that the device can be designed to efficiently perform a filter function.

The structure studied can be used for modulators, displayers, color extraction for imaging, etc. For an example of amplitude modulator application, the voltage can be set as $(80 + 20\cos\Omega t)$ V, where the bias is 80 V and the signal is $(20\cos\Omega t)$ V. Then, the wavelength of the carrier wave can be set as the resonance wavelength of the structure for 60 V. As a result, the amplitude of the reflected light will be $A(t) = A_0 + A_1\cos\Omega t$, which carries the information of the voltage signal. It should be noted that the wavelength of the carrier light should be the resonance wavelength at the applied voltage of 60 V, not 80 V. From Fig. 7 it can be seen that a small change in the signal voltage can cause a sharp change in the strength of a reflected wave due to the motion of the spectrum; therefore, small signals can cause deep modulation. For an example of color displayers, we need to set up three basic filters with the wavelengths of red, green, and blue lights and use the color signal voltage to tune the reflection strength in each pixel, and the reflected lights display the right color images.

To understand the results shown in Section 3, here we present a theoretical analysis. As the metasurface is periodic, and there is plasmonic response in the gold nanospheres under the action of the incident light wave, the excited waves along the surface can be regarded as a standing wave with a wavelength of $\lambda = d/\mathrm{Re}(n_I)$, corresponding to an angular frequency of $2\pi[C/\mathrm{Re}(n_I)]/\lambda = 2\pi C/d$, where $\mathrm{Re}(n_I)$ is the real part of the effective refractive index n_I of the material, including the gold nanoshpere region and the EO material layer, C is the speed of light in free space. Noting that one can regard a number of unit cells as a supercell without changing the property of the metasurface, there also exist standing waves with periods of qd, where q is an integer greater than 1. Similarly, we can write out the angular frequency of the standing waves as

$$\omega = 2\pi C/(qd). \tag{5}$$

Moreover, the gold nanospheres respond strongly to incident waves; therefore, the region with the gold nanospheres has good reflectance to waves and can server as a good mirror. Also, the gold substrate layer is a perfect mirror, so a Fabry–Perot resonator is formed by the nanosphere layer and the substrate sandwiched by the EO layer. As is known, there is some loss due to the gold nanospheres, so the Fabry–Perot resonance will cause resonant absorption. The effective dielectric constant in the direction along the metasurface for the effective medium originated from the nanosphere layer and the EO layer can be written as

$$\varepsilon_{rI} = (d^2h_1 + d^2h_2)^{-1} \times (d^2h_1 - 4\pi r^3 + 4\pi r^3\varepsilon_{rAu} + d^2h_2\varepsilon_o), \tag{6}$$

where r, d, h_1, h_2, ε_{rAu}, and ε_o are the radius of the nanoshperes, the lattice constant of the unit cell in the metasurface, the thicknesses of layer with nanospheres and the EO layer, the dielectric constant of the gold, and the ordinary dielectric constant of the EO material, respectively. From the above equation, we can obtain the effective refractive index as $n_I = \sqrt{\mathrm{Re}(\varepsilon_{rI}) + i\mathrm{Im}(\varepsilon_{rI})}$.

Then, we can write out the Fabry–Perot resonance condition due to the nanoshpere layer and the gold substrate layer as

$$\mathrm{Re}(n_I)(\delta + h_2) = p\lambda/2 = \pi pC[\omega\mathrm{Re}(n_I)], \tag{7}$$

where δ is the distance from the upper surface of the EO layer to the effective reflecting surface in the nanosphere region, λ is the free-space wavelength of the incident wave, and p is the mode number, which is an integer. Considering that most of the waves are below the balls, it is reasonable to have $\delta = r/2 = 6$ nm.

For $r \ll d$ and $\omega_p \gg \omega$, the resonance condition is reduced to be

$$\omega^5 + c_1\omega^4 + c_2\omega^3 + c_3 = 0, \tag{8}$$

where $c_1 = -\pi pC(h_1 + h_2)/[(\delta + h_2)(h_1 + h_2\varepsilon_o)]$, $c_2 = -4\pi r^3 d^{-2}\omega_p^2/(h_1 + h_2\varepsilon_o)$, and $c_3 = 4\pi p^{-1}C^{-1}r^6 d^{-4}\gamma^2\omega_p^4(\delta + h_2)/[(h_1 + h_2\varepsilon_o)(h_1 + h_2)]$.

For $d = 100$ nm, $r = 12$ nm, $h_1 = 24$ nm, $h_2 = 70$ nm, $\delta = r/2 = 6$ nm, $\omega_p = 1.37 \times 10^{16}$ rad/s, $V = 80$ V, $n_o = 2.34$, $\varepsilon_o = n_o^2 = 5.4756$, $\gamma = 1.23 \times 10^{14}$ rad/s, and $p = 1$, we can obtain the nontrivial solutions of the equation to be $\omega_1 = 3.1134 \times 10^{15}$ rad/s whose free-space wavelength is $\lambda_1 = 605.01$ nm. The corresponding wavelength obtained by FEM shown in Fig. 9 is 610 nm for $V = 80$ V, indicating a relative difference between the results obtained by FEM and the simple analytical theory of 0.82%.

It is natural that the system will have strong resonance when the wavelength of the standing wave on the metasurface is approximately equal to Fabry–Perot resonance wavelength. Then, from the above results, we can see that it is the strong coupling between the sixth-order standing wave ($\omega = 2\pi C/(6d) = 3.1394 \times 10^{15}$ rad/s or free-space wavelength of 600 nm) and the fundamental Fabry–Perot resonance mode [605.01 nm obtained from Eq. (8)] in the structure responsible for the filtering property of the structure, which has a strong absorption at 605.01 nm, as can be seen in Fig. 7.

Moreover, from Eqs. (2) and (6)–(8), $E = V/h_1$, and $\varepsilon_o = n_o^2$, we can see that the resonance condition and thus the filtering wavelength, i.e., the antireflecting wavelength, can be tuned by the applied voltage V. However, the tuning range is limited both by the voltage breakdown of the EO material layer and by the requirement that the wavelength of standing wave on the metasurface should be approximately equal to the Fabry–Perot resonance wavelength.

5. CONCLUSION

In this paper, a tunable antireflection plasmonic filter in the visible near-infrared range is proposed on the basis of an MDM structure, in which an array of gold nanospheres was placed on the top layer. The tunability was obtained by the insertion of $LiNbO_3$ as a dielectric. The optical spectra are derived by an FEM simulation tool and have shown that the wavelength of resonance peaks can be controlled by modulating the refractive index of a dielectric exploiting the Pockels effect. It is found that the frequency of the plasmonic resonance wave on the metasurface should be equal to that of the Fabry–Perot resonator formed by the MDM to have a good filtering property. The results obtained and the nature of the designed structure ensures the feasibility of a tunable antireflection narrowband filter for optical integrated circuits [32]. Our simple analytical theory agrees with the FEM simulation results in high precision.

Funding. National Natural Science Foundation of China (NSFC) (61275043, 61605128, 61307048).

REFERENCES

1. M. Qi, E. Lidorikis, P. T. Rakich, S. G. Johnson, J. D. Joannopoulos, E. P. Ippen, and H. I. Smith, "A three-dimensional optical photonic crystal with designed point defects," Nature **429**, 538–542 (2004).
2. D. K. Gramotnev and S. T. Bozhevolnyi, "Plasmonic beyond the diffraction limit," Nat. Photonics **4**, 83–91 (2010).
3. M. E. Stewart, C. R. Aenderton, L. B. Thompson, J. Maria, S. K. Gray, J. A. Rogers, and R. G. Nuzzo, "Nanostructure plasmonic sensors," Chem. Rev. **108**, 494–521 (2008).
4. E. Ozbay, "Plasmonics: merging photonics and electronics at nanoscale dimensions," Science **311**, 189–193 (2006).
5. W. E. Lai, H. W. Zhang, Y. H. Zhu, Q. Y. Wen, W. W. Du, and X. L. Tang, "A bilayer metallic nanofilms in broadband antireflection in terahertz optical systems," Opt. Express **22**, 2174–2184 (2014).
6. E. Laux, C. Genet, T. Skauli, and T. W. Ebbeson, "Plasmonic photon sorters for spectral and polarimetric imaging," Nat. Photonics **2**, 161–164 (2008).
7. K. Diest, J. A. Dionne, M. Spain, and H. A. Atwater, "Tunable color filters based on metal-insulator-metal resonators," Nano Lett. **9**, 2579–2583 (2009).
8. R. Bandyopadhyay and R. Chakraborty, "Design of tunable transmission filter using one-dimensional defective photonic crystal structure containing electro-optic material," Opt. Eng. **54**, 117105 (2015).
9. H. Lu, X. Liu, D. Mao, L. Wang, and Y. Gong, "Tunable bandpass plasmonic waveguide filters with nanodisk resonators," Opt. Express **18**, 17922–17927 (2010).
10. Y. J. Liu, Y. B. Zheng, J. Loou, I. K. Chiang, I. C. Khoo, and T. J. Huang, "All-optical modulation of localized surface plasmon coupling in hybrid system composed of photon-switchable gratings and Au nanodisk array," J. Phys. Chem. C **115**, 7717–7722 (2011).
11. S. Sun, Q. He, S. Xiao, Q. Xu, X. Li, and L. Zhou, "Gradient-index meta-surfaces as a bridge linking propagating waves and surface waves," Nat. Mater. **11**, 426–431 (2012).
12. X. Chen, L. Huang, H. Mühlenbernd, G. Li, B. Bai, Q. Tan, G. Jin, C.-W. Qiu, S. Zhang, and T. Zentgraf, "Dual-polarity plasmonic metalens for visible light," Nat. Commun. **3**, 1198 (2012).
13. H. F. Ma, G. Z. Wang, G. S. Kong, and T. J. Cui, "Independent controls of differently-polarized reflected waves by anisotropic metasurfaces," Sci. Rep. **5**, 9605 (2015).
14. X. Ni, A. V. Kildishev, and V. M. Shalaev, "Metasurface holograms for visible light," Nat. Commun. **4**, 2807 (2013).
15. G. Zheng, H. Mühlenbernd, M. Kenney, G. Li, T. Zentgraf, and S. Zhang, "Metasurface holograms reaching 80% efficiency," Nat. Nanotechnol. **10**, 308–312 (2015).
16. H. X. Xu, S. Tang, S. Ma, W. Luo, T. Cai, S. Sun, Q. He, and L. Zhou, "Tunable microwave metasurfaces for high-performance operations: dispersion compensation and dynamical switch," Sci. Rep. **6**, 38255 (2016).
17. G. M. Wang, H. X. Xu, J. Xiao, T. Cai, and Y. Q. Zhuang, "Tunable Pancharatnam-Berry metasurface for dynamical and high-efficiency anomalous reflection," Opt. Express **24**, 27836–27848 (2016).
18. H. X. Xu, S. Ma, W. Luo, T. Cai, S. Sun, Q. He, and L. Zhou, "Aberration-free and functionality-switchable meta-lenses based on tunable metasurfaces," Appl. Phys. Lett. **109**, 193506 (2016).
19. H. X. Xu, S. Sun, S. Tang, S. Ma, Q. He, G. M. Wang, T. Cai, H. P. Li, and L. Zhou, "Dynamical control on helicity of electromagnetic waves by tunable metasurfaces," Sci. Rep. **6**, 27503 (2016).
20. J. Park, H. Kim, and B. Lee, "High order plasmonic Bragg reflection in the metal-insulator-metal waveguide Bragg grating," Opt. Express **16**, 413–425 (2008).
21. Y. Gong, L. Wang, X. Hu, X. Li, and X. Liu, "Broad-bandgap and low-sidelobe surface Plasmon polariton reflector with Bragg-grating based MIM waveguide," Opt. Express **17**, 13727–13736 (2009).
22. L. Domeash, M. Wu, N. Nemchuk, and E. Ma, "Tunable and switchable multiple cavity thin film filter," J. Lightwave Technol. **22**, 126–135 (2004).

23. M. A. Swillam and R. K. Y. Ismail, "Tunable nanoplasmonics," Adv. Electromagn. **2**, 1–5 (2013).
24. M. Xiao and N. Rakov, "Surface propagation with large spectral red-shift on a gold thin film containing subwavelength holes," Phys. Lett. A **309**, 452–456 (2003).
25. U. Kreibig and P. Zacharias, "Surface plasmon resonances in small special silver and gold particles," Z. Phys. **231**, 128–143 (1970).
26. T. Volk and M. Wohlecke, "Lithium Niobate: defects, photorefraction and ferroelectric switching," Springer Ser. Mater. Sci. **115**, XIV–250 (2009).
27. M. Aufray, S. Menuel, Y. Fort, J. Eschbach, D. Rouxel, and B. Vincent, "New synthesis of nanosized niobium oxides and lithium niobate particles and their characterization by XPS analysis," J. Nanosci. Nanotechnol. **9**, 4780–4785 (2009).
28. Q. Zhu and Y. Zhang, "Defect modes and wavelength tuning of one dimensional photonic crystal with lithium niobate," Optik **120**, 195–198 (2009).
29. C. Manolatou, M. J. Khan, S. Fan, P. R. Villenueve, H. A. Haus, and J. D. Joannopoulos, "Coupling of modes analysis of resonant channel add-drop filters," J. Quantum Electron. **35**, 1322–1331 (1999).
30. S. A. Maier, "Plasmonic field enhancement and SERS in the effective mode volume picture," Opt. Express **14**, 1957–1964 (2006).
31. A. F. M. Y. Haider, S. Sengupta, K. M. Abedin, and A. I. Talukder, "Fabrication of gold nanoparticles in water by laser ablation technique and their characterization," Appl. Phys. A **105**, 487–495 (2011).
32. H. Zhang, Y. Betremieux, J. Noto, and R. Kerr, "Novel tunable liquid crystal Fabry-Perot filters for fiber-optical system," Proc. SPIE **4583**, 4564–4572 (2001).